CHEMIJA. 2017. Vol. 28. No. 2. P. 85–92
© Lietuvos mokslų akademija, 2017

Synthesis, structure and photoelectrochemical behaviour of ZnO coatings on AISI 304 type steel

Agnė Šulčiūtė*,

Simona Ostachavičiūtė,

Eugenijus Valatka

Department of Physical and Inorganic Chemistry, Kaunas University of Technology, Radvilėnų Rd. 19, LT-50254 Kaunas, Lithuania

ZnO nanoparticles were prepared by thermal decomposition of precursor zinc acetate. Using electrophoretic deposition (EPD) ZnO coatings on AISI 304 steel were formed. The optimum deposition conditions for ZnO coatings were experimentally determined. The effects of synthesis conditions on the structure, morphology, composition and electrochemical properties of deposited coatings were studied by differential scanning calorimetry and thermogravimetry (DSC–TG) analysis, X-ray diffraction (XRD), Fourier-transform infrared (FTIR) analysis and photo-voltammetry. The photoelectrochemical performance of the prepared ZnO films was evaluated in a 0.1 M Na_2SO_4 aqueous solution. Also, the as-prepared photocatalysts were modified with a cobalt-based (Co–P_i) oxygen evolving catalyst (OEC) using photo-assisted deposition. The voltammetric characteristics revealed that the presence of a cobalt-based catalyst effectively changes the photoelectrocatalytic activity of oxide particles.

Keywords: zinc oxide, electrophoretic deposition, photoelectrochemical, cobalt phosphate

INTRODUCTION

Transition metal oxides have been widely studied due to their good electrocatalytic activity for many types of electrode reactions such as oxygen or hydrogen evolution, oxygen reduction and organic electrosynthesis. Particular attention is paid to the search of efficient and low-cost electrocatalysts suitable for the implementation of the water photo-splitting process. In this regard, zinc oxide (ZnO) is a material of prime choice. It is widely used in various industrial applications, such as catalysts, rubber and concrete additives, photovoltaics, pigments, gas sensors and mixed oxide varistors [1–5]; however, its use in aqueous photoelectrochemical systems is hindered by rather fast photocorrosion [6]. In order to overcome this drawback, recent research efforts have been systematically focused on the improvement of ZnO stability and catalytic properties by enhancing the performance and modificating the surface with an oxygen evolving catalyst (OEC) [7, 8]. Recently, inorganic cobalt–phosphate complex (termed Co–P_i) has emerged as a particularly promising OEC based on earth-abundant elements.

ZnO can be deposited by using a number of methods, specifically: chemical vapour deposition, radio frequency magnetron sputtering, molecular beam epitaxy, sol–gel, hydrothermal synthesis, electrophoretic and electrochemical deposition. The electrophoretic deposition (EPD) is a cost-competitive technique for obtaining highly uniform films with the thickness ranging within the nanometer-to-micrometer scale by altering the applied voltage and the deposition time. The main advantages of the EPD method are as follows [9, 10]: it can be applied to any available solid material in the form of fine powder, rapid film deposition, low cost, simple instrumentation, minor restriction on the shape of substrates, good potential for the conservation of materials. EPD has been reported to be a highly beneficial technique for the preparation of nanostructured ZnO films [10–22]. Both aqueous and non-aqueous ZnO suspensions have been used for the coating of various substrates (transparent conductive oxide glass, anodic alumina membranes, steel and nickel). Methanol, ethanol, propanol, isopropyl alcohol, etc. were used as solvents.

* Corresponding author. E-mail: agne.sulciute@ktu.lt

The research of scholarly writings showed that the nature of the starting material and synthesis conditions are important for the ZnO photocatalyst activity. Depending on the ZnO treatment conditions the coatings of various structures, morphology, composition and photoactivity may be obtained. To the best of our knowledge, there is no published data concerning the electrophoretic deposition of ZnO on the stainless steel substrate when using thermally decomposed zinc acetate dehydrate. The aim of the work was to synthesize ZnO and ZnO/Co–P_i coatings on stainless steel and to investigate their structure and electrochemical properties.

MATERIALS AND METHODS

Formation of ZnO coatings

All reagents used in the experiments were chemically or analytically pure commercial reagents. Zinc acetate dihydrate ($Zn(CH_3COO)_2 \cdot 2H_2O$, >97% purity) obtained from Reachim (Russia) served as the precursor for the synthesis of bare ZnO powder. 0.5 g of the precursor was placed in a porcelain crucible, covered by an aluminum lid, and heat-treated at 673 K for 1 hour under atmospheric conditions [23].

AISI 304 type stainless steel plates 0.5 mm thick were used as an electroconductive support. According to the manufacturer, the composition of stainless steel is as follows (wt.%): C, 0.08; Cr, 18–20; Ni, 8–10.5; Mn, 2.0; Si, 1.0; P, 0.045; S, 0.03; Fe, the balance.

The suspension for the electrophoretic deposition (EPD) was prepared by dispersing 2 g of the prepared ZnO powder in 100 mL of methanol (CH_3OH, Lachema, Czech Republic, 99.5% purity). A homogenous suspension was achieved under vigorous stirring for 10 min. Two stainless steel plates (5 × 1 cm each) were immersed into the prepared suspension of ZnO. The distance between the anode and the cathode was 2 cm. EPD synthesis was performed under constant voltage (10–40 V) and was controlled using a DC power supply B5-49 (MNIPI Inc., Russia). The deposition time varied in the range of 0.5–40 min. The formation of ZnO coatings took place on the cathode. In order to achieve better adhesion of ZnO particles on the stainless steel substrate, all the samples were thermally treated at 673 K for 1 hour in the atmospheric air.

Photochemical deposition of Co–P_i catalyst

Experimental runs were performed by using a photochemical reactor. The prepared photoanode (ZnO on stainless steel) was immersed in 50 mL of a mixture containing 0.1 M phosphate buffer (pH 7) and 0.5 mM cobalt nitrate ($Co(NO_3)_2 \cdot 6H_2O$, >99%, Chempur, Poland). The mixture was vigorously stirred at 298 K and was irradiated with a 400 W HPA 400/30S (Philips, The Netherlands) high pressure metal halogen lamp up to 40 min. The lamp was held at 2 cm from the reactor. An emission spectrum of this lamp is characterized by its high radiation intensities in the 300–400 nm wavelength range (the maximum intensity of the lamp radiation is $9.03 \cdot 10^{18}$ photons $\cdot$ s^{-1}) [24].

Analytical techniques

Differential scanning calorimetry and thermogravimetry (DSC–TG) analysis was performed on a Netzsch STA 409 PC Luxx (Netzsch GmbH, Germany) simultaneous thermal analyzer. Analytical parameters were the following: the rate of temperature increase was 15° $\cdot$ min^{-1}; the temperature range was set at 303–773 K; a blank Pt/Rh crucible was used; the heating was carried out in the atmospheric air.

Fourier transform infrared (FT-IR) spectra were obtained on a Perkin Elmer FT-IR Spectrum X System while using KBr pellets. 1 mg of the substance was mixed with 200 mg of KBr, and these pellets were pressed in vacuum environment. The scanning range was 400–4000 cm^{-1}, whereas the resolution was 1 cm^{-1}.

The surface morphology and the composition of ZnO powder were investigated with a Quanta FEG 200 (FEI) high resolution scanning electron microscope (SEM). The images were obtained at 20–30 kV, the pressure in the chamber was set at 80 Pa, up to ×150 000 magnification was employed depending on the sample. The samples were imaged without any conductive coating. SEM was equipped with a Bruker XFlash® 4030 detector (Bruker AXS) for high resolution energy dispersive X-ray spectroscopy (EDX).

X-ray powder diffraction (XRD) data were collected with a DRON-6 (Bourevestnik Inc., Russia) powder diffractometer equipped with Bragg–Brentano geometry and using Ni-filtered CuK_α radiation and a graphite monochromator. The crystallite size D_{hkl} was calculated from the line broadening using the Scherrer's equation [25]

$$D_{hkl} = \frac{k \cdot \lambda}{B_{hkl} \cdot \cos\theta}, \quad (1)$$

where λ is the wavelength of the CuK_α radiation ($1.54056 \cdot 10^{-10}$ m), θ is the Bragg diffraction angle, B_{hkl} is the full width at the half-maximum intensity of the characteristic reflection peak ($2\theta = 31.66°, 34.38°, 36.26°$ for ZnO). Here k is the constant (the value of 0.94 was used in this study).

The pH was measured by using a 673 M pH meter.

Electrochemical measurements were performed by a computer-controlled Autolab PGSTAT12 (Ecochemie, The Netherlands) potentiostat/galvanostat using a standard three electrode cell (volume 100 mL). The GPES® 4.9 software was used for the collection and treatment of the experimental data. All the potentials are referred to the Ag, $AgCl|KCl_{(sat)}$ reference electrode. Throughout the paper, all the potentials are referred to this electrode. The cathodic compartment housed a platinum wire (geometric area about 15 cm^2) as a counter electrode. The working electrode was AISI 304 stainless steel.

The photoelectrochemical activity of the prepared electrodes was investigated by employing photovoltammetry measurement methods. A photoelectrochemical quartz cell was employed. Phosphate buffer or 0.1 M Na_2SO_4 (>99%, Reachim, Russia) solutions, both of pH 7, were used as the supporting electrolytes. A phosphate buffer of pH 7 was prepared by using the following procedure: 61.5 ml of K_2HPO_4 (>98%, Reachim, Russia) and 38.5 ml KH_2PO_4 (>98%, Reachim, Russia) of 1 M stock solutions were combined and then diluted to obtain 1 litre solution; distilled water was added. A phosphate buffer of pH 11.5 was prepared by using the following procedure: 100 ml of 0.05 M K_2HPO_4 (>98%, Reachim, Russia) and 22.2 ml 0.1 M NaOH (>98%, Reachim, Russia) stock solutions were combined and then diluted to 200 ml with the addition of distilled water. Solutions were not stirred during all the photoelectrochemical activity measurements.

In the case of the stainless steel substrate, the back side of the working electrode was insulated with epoxy resin in order to eliminate its contribution to the dark current. The coated area of the electrode was carefully positioned in the path of the UV irradiation. A General Electric F8W/BLB lamp (λ_{max} = 366 nm, the average power density being 1.8 mW cm^{-2} [24]) was placed at a distance of 2 cm from the working electrode and was used as an UV radiation source.

The incident photon-to-current efficiency (IPCE) value of the photoelectrode was calculated by using the following relation [26]

$$\mathrm{IPCE}\,(\%) = 100\frac{1240 \cdot j_{ph}}{\lambda \cdot P}, \qquad (2)$$

where j_{ph} is the photocurrent density in mA · cm^{-2}, λ is the wavelength of the incident light in nanometers (the value used in this study was 366 nm), and P is the incident light intensity in mW · cm^{-2}.

The photocurrent of the coatings modified with $Co–P_i$ were measured in a three-electrode setup by using a 0.1 M potassium phosphate electrolyte (pH 11.5). A pH 11.5 medium was chosen because the ZnO electrode is chemically and photochemically the most stable at pH ~12 [27].

RESULTS AND DISCUSSION

Structural and morphological characterization of ZnO powder

The synthesis of bare ZnO powder was carried out by thermal decomposition of zinc acetate. Thermogravimetric (TG) and differential scanning calorimetry (DSC) analyses were performed in order to determine the thermal effects during the decomposition of zinc acetate in the atmospheric air (Fig. 1).

The first mass loss of 14.19% prior to reaching the temperature of up to 400 K was accompanied by an endothermic peak at 373 K. This corresponds to the theoretical value of the thermal dehydration of two water molecules (16.41%) [23, 28]:

$$Zn(CH_3COO)_2 \cdot 2H_2O\,(s) \rightarrow Zn(CH_3COO)_2\,(s) + 2H_2O\,(g).$$

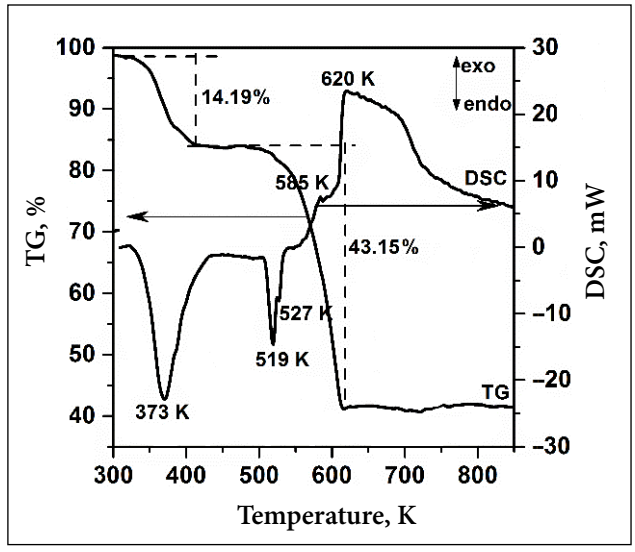

Fig. 1. TG-DSC pattern of zinc acetate

After dehydration, the mass loss was 43.15 % and it can be assigned to the decomposition of anhydrous $Zn(CH_3COO)_2$ into ZnO. The endothermic peak value at 519 K is close to the melting point of anhydrous zinc acetate and has a shoulder at 527 K. Consequently, it is suggested [23] that two different compounds coexisted in the specimen when heated at rapid heating rate conditions. During the decomposition of zinc acetate, anhydrous zinc acetate is believed to oligomerize on sublimation and to form basic zinc acetate, $ZnO_4(CH_3COO)_6$, which is a favourable precursor for the formation of ZnO coatings [23, 28]:

$$4Zn(CH_3COO)_2\,(s) \rightarrow Zn_4O(CH_3COO)_6\,(s) + (CH_3CO)_2O\ (g),$$

$$Zn_4O(CH_3COO)_6\,(s) \rightarrow 4\,ZnO\,(s) + 3\,CH_3COCH_3\,(g) + 3\,CO_2\,(g).$$

The total mass loss reaches 57.34%, and ZnO was found to be the main residue.

The DSC curve indicated one exothermic peak at 620 K with a shoulder at 585 K; thus it may be related to the removal of residual organics (acetate, CO_2) [23, 28].

The XRD analysis reveals the diffraction peaks at 2θ = 31.78°, 34.44° and 36.24° (Fig. 2) which correspond to the well-crystallized wurtzite-type ZnO (PDF 04-004-4120). According to the Scherrer's equation (1), the average ZnO crystallite size was calculated to be 35.3 nm.

ZnO powder was also investigated by infrared absorption analysis (Fig. 3). The large absorption band centered at 3447 cm^{-1} can be assigned to the stretches of hydroxy groups. The peak observed at 2945 cm^{-1} represents the C–H bond thus indicating aliphatic hydrocarbon asymmetrical stretching [29]. The other distinct peak at the wavenumber of 2355 cm^{-1} indicates –COO. 1589 cm^{-1} can be attributed to the asymmetrical

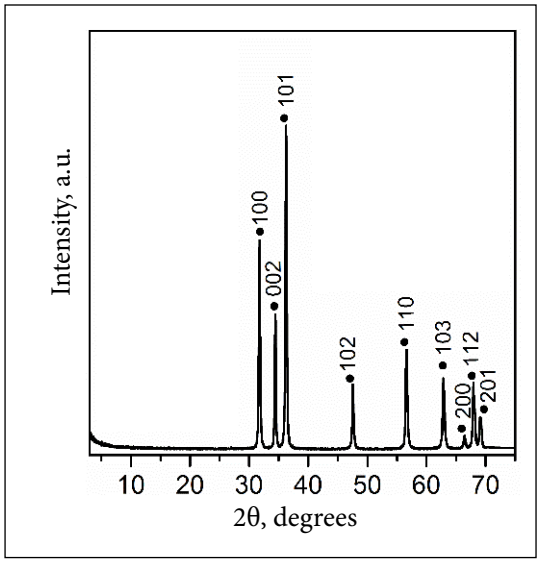

Fig. 2. XRD pattern of ZnO obtained by thermal decomposition of zinc acetate dihydrate at 673 K

stretching vibrations of the acetate ions and is associated with the C=O bond. Other peaks at 1340 cm^{-1} show the presence of CH_3 groups [30]. The band at 880 cm^{-1} corresponds to the carbonate ion vibration. A broad band centered at 495 cm^{-1} corresponds to the characteristic stretching of the Zn–O bond, and it can be used for the identification of zinc (white pigment) in the IR spectra of real paint sample layers [31].

Figure 4 presents the morphological characteristics of the prepared ZnO powder. It is seen that the flower-like structure is formed, which consists of a variety of building blocks, mainly rods. These results are in agreement with those presented in [23].

The formation of ZnO coatings on the AISI 304 type stainless steel substrate was implemented by electrophoretic deposition. The preliminary experimental runs revealed that the most uniform and stable ZnO coatings are obtained when the applied potential between electrodes is 30 V. Figure 5 shows the experimental results of the deposited ZnO weight as a function of electrophoresis time. It is prominent that the amount of

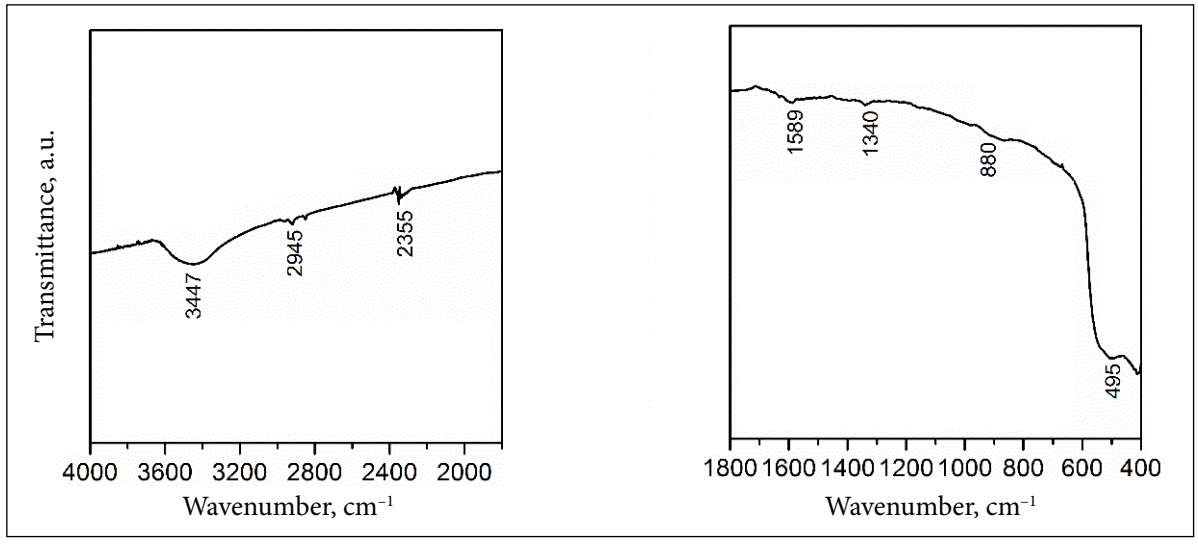

Fig. 3. FT-IR spectrum of ZnO obtained by thermal decomposition of zinc acetate dihydrate at 673 K

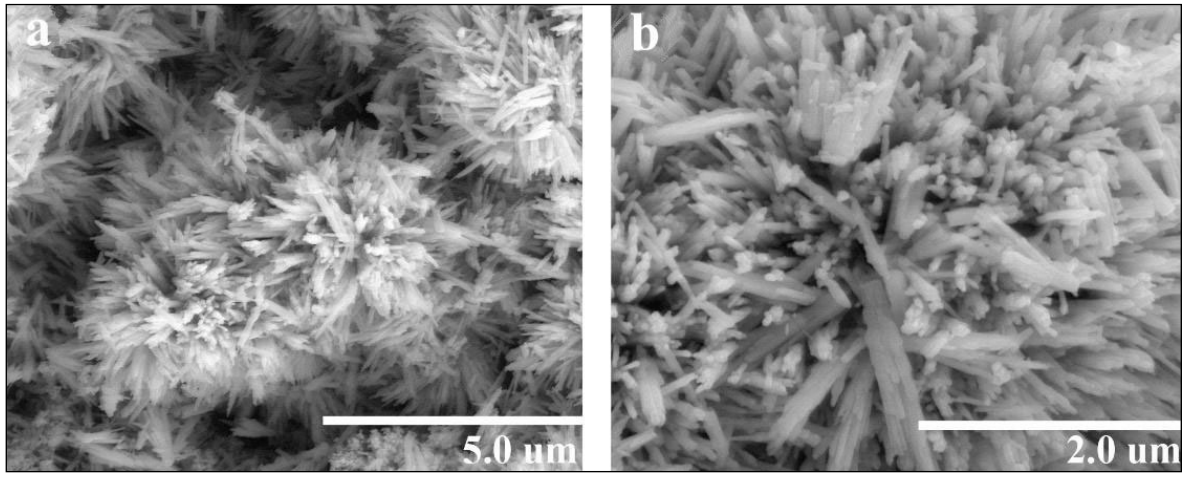

Fig. 4. SEM images of ZnO obtained by thermal decomposition of zinc acetate dihydrate at 673 K at various magnifications: (a) ×20 000, (b) ×50 000

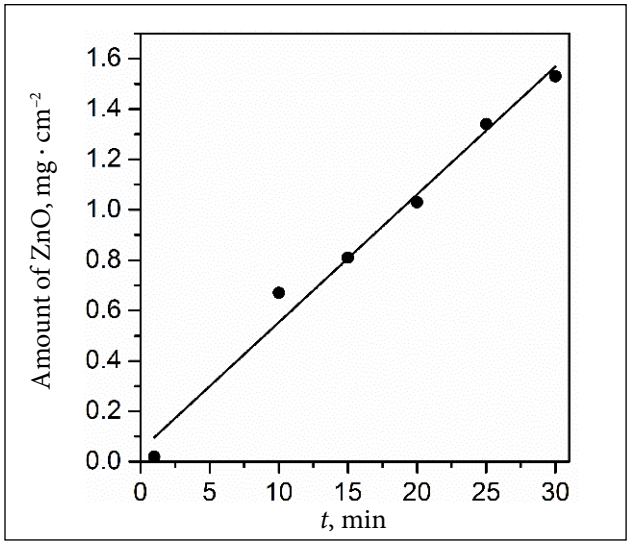

Fig. 5. The amount of immobilized ZnO as a function of electrophoretic deposition time *t*

the deposited ZnO increases almost linearly with the increase in deposition time. Moreover, it was observed that the rate of ZnO deposit formation increases together with the increase in the applied voltage. However, it is well documented [32] that the quick formation of particulate coatings on the electrode can result in poorer deposit quality as the accumulation rate of the particles greatly influences their packing behaviour in coatings.

Photoelectrochemical behaviour of ZnO coatings

The photoelectrochemical behaviour of the ZnO electrode (30 V, deposition time 20 min) was determined from the current–potential curves obtained in 0.1 M Na_2SO_4 solutions both in the dark and under UV irradiation (Fig. 6). The potential was swept from –0.3 V to +1.0 V at 10 mV · s^{-1}. It is evident that the UV irradiation caused a significant increase in the observed current. Such a behaviour is characteristic of *n-type* semiconducting materials and is related to photogenerated electron diffusion through the catalyst coating towards the cathode [33]. The observed anodic photocurrent can be related to the generation of hydroxyl radicals (HO•) and other oxidation products (e.g. H_2O_2) at the surface of the ZnO electrode. The presence of HO• radicals at the interface of the ZnO/aqueous solution was confirmed with the help of the radical-trapping technique. Hydrogen peroxide is formed as a result of the interaction of generated hydroxyl radicals [34]:

$$ZnO + h\nu \rightarrow e^- + h^+, \quad (3)$$

$$h^+ + HO^- \rightarrow HO^\bullet, \quad (4)$$

$$h^+ + H_2O \rightarrow H^+ + HO^\bullet, \quad (5)$$

$$e^- + O^2 \rightarrow O_2^{\bullet -}, \quad (6)$$

$$O_2^- + H^+ \rightarrow HO_2^\bullet, \quad (7)$$

$$2\,HO_2^\bullet \rightarrow O_2^{\bullet -} + H_2O_2, \quad (8)$$

$$H_2O_2 + O_2^{\bullet -} \rightarrow HO^\bullet + HO^- + O_2. \quad (9)$$

The rate of hydrogen peroxide formation in aerated ZnO aqueous suspensions is highly dependent on the presence of various organic and inorganic species [34]. It should be emphasized that at the same time the photodissolution (photocorrosion) of ZnO takes place to some extent due to the self-oxidation through photohole generation [35].

The time dependence of the electrode potential and the current density in the dark and under UV irradiation

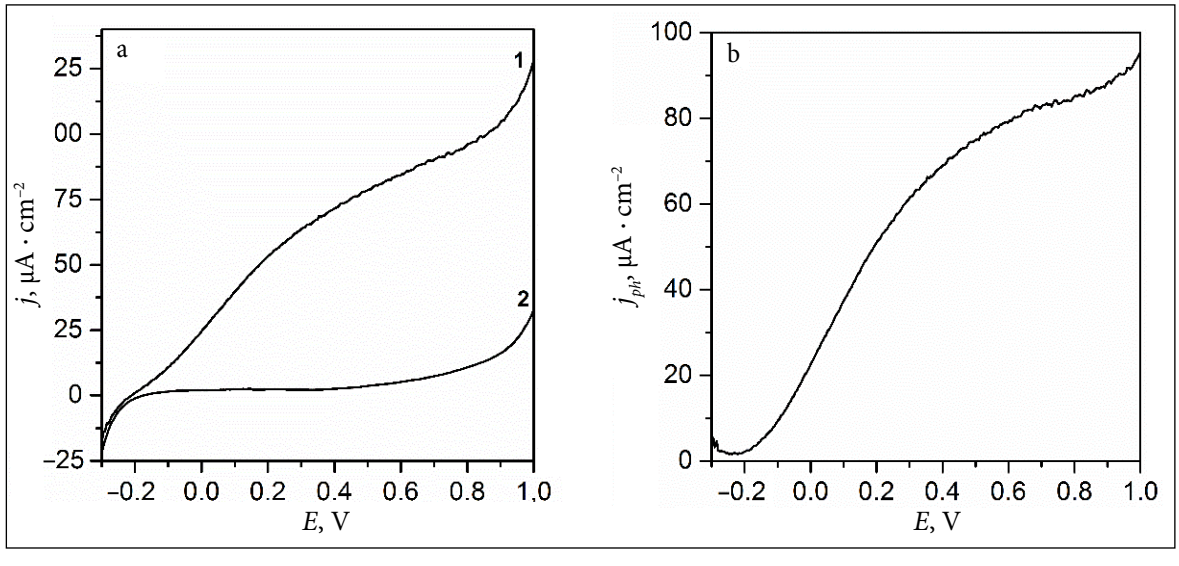

Fig. 6. (a) Characteristic voltammograms in the dark (2) and under UV illumination (1) of the ZnO electrode. The potential scan rate $v = 10$ mV · s^{-1}, 0.1 M Na_2SO_4; the supporting electrolyte at 291 K. (b) Plot of the photocurrent density, j_{ph}, with respect to the applied potential, *E*

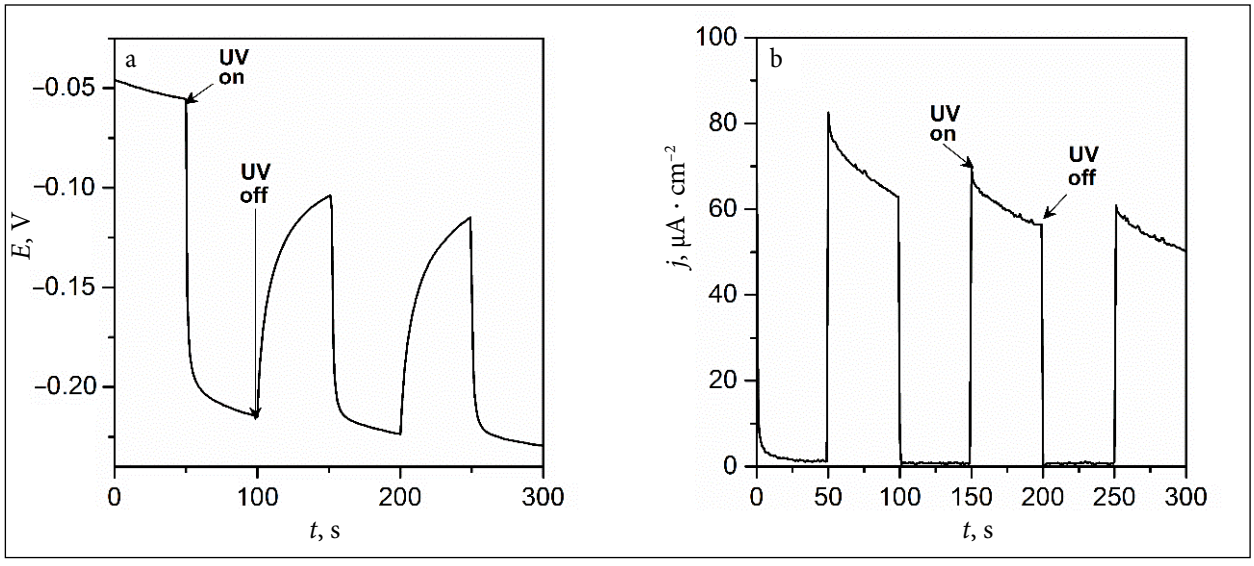

Fig. 7. Variation of the open circuit potential (a) and the current density at +0.6 V (b) for ZnO electrode in 0.1 M Na_2SO_4 solution in the dark and under UV illumination

for the ZnO electrode is presented in Fig. 7. When the light was switched on, the observed potential jumped to –0.24 V. The observed decrease in the potential can be explained by the fact that the photoholes react rapidly with water molecules while the photoelectrons accumulate on the surface of ZnO particles and charge them negatively. Under UV irradiation, the observed current jumped to about 87 μA · cm^{-2} (Fig. 7b). When the light was switched off, the current of the ZnO electrode decreased and equalled its initial value.

The results presented in the Table confirmed that the photoelectrochemical activity of the prepared electrodes is dependent on the amount of immobilized ZnO. The incident photon-to-current efficiency (IPCE) value of a photoelectrode was evaluated by using Eq. 2. Photocurrent densities are calculated for the +0.6 V potential because at higher potential values the current increase may be associated with stainless steel dissolution and oxygen evolution [36].

The obtained results show that the 1.03 mg · cm^{-2} loading of ZnO gives the largest photocurrent and, consequently, the highest IPCE value. At a higher ZnO loading the photocurrent tends to decrease. Such dependence is a result of the interplay of various parameters, for instance, the intensity of incident irradiation and the interconnection of ZnO particles in the coating. It is known [37] that there is an optimal layer of thickness if the potentially highest IPCE values are required to be reached. At higher oxide loadings, only the part of the semiconductor layer can be efficiently irradiated with UV light. It means that the nonactive layers of the semiconductor can exist near the surface of the electrode. This layer can act as a recombination zone for the photogenerated charge carriers.

It should be pointed out that in this work efforts were made in order to optimize the thickness of the ZnO coatings in terms of their photoactivity. It was discovered that the highest photocurrent (up to 100 μA · cm^{-2}) can be generated in the case of thin coatings (~0.18 μm). However, the formation of very thin uniform and reproducible coatings when using electrophoretic deposition presents some technical difficulties. In addition, the electrochemical measurements revealed that the photostability of such ZnO coatings is rather poor.

Influence of Co–P_i catalyst on photoelectrochemical properties of ZnO

The analysis of literature data revealed that the photoelectrochemical performance of oxide semiconductors

Table. **Influence of the amount of ZnO on the photoelectrochemical activity of the prepared electrodes**

Deposition time, min	Amount of the deposited ZnO, mg · cm^{-2}	Average thickness of the ZnO layer, μm	Photocurrent density j_{ph} at +0.6 V, μA · cm^{-2}	IPCE, %
10	0.77	0.41	41.5	7.8
15	0.81	0.45	43.0	8.1
20	1.03	0.57	77.9	14.6
25	1.34	0.70	43.1	8.1
30	1.53	0.82	46.4	8.7

can be enhanced by coupling them with a cobalt-based oxygen-evolving catalyst (termed Co–P_i) in phosphate electrolytes. That is why in the present paper the influence of the Co–P_i catalyst on the photoelectrochemical activity of the prepared ZnO electrodes was tested. Electrophoretically deposited ZnO coatings on AISI 304 steel were used as a support for the Co–P_i catalyst. The photoelectrochemical characterization of ZnO/Co–P_i coatings was carried out by using pH 11.5 phosphate solutions, also taking into account the fact that ZnO was established to be the most photochemically stable substance in this pH [27]. On the other hand, the presence of phosphate ions is essential for the stability of the Co–P_i catalyst.

The Co–P_i catalyst was deposited photochemically by immersing the ZnO electrode in the 0.1 M phosphate buffer (pH 7) with 0.5 mM cobalt nitrate and by irradiating the sample with UV light for various periods of time. The proposed mechanism [27, 38] demonstrated that the photogenerated holes possess sufficient overpotential to oxidize Co^{2+} to Co^{3+} ions in order to form the Co–P_i catalyst. During the process of photodeposition, the generated photoelectrons are consumed by the reduction of water or by the dissolved oxygen.

The linear sweep voltammetry in the dark and under UV irradiation was used to evaluate the influence of the Co–P_i catalyst on the photoelectrochemical performance of the ZnO coatings. The obtained experimental results are summarized in Fig. 8. It was established that the presence of the Co–P_i catalyst on the surface of ZnO results in the decrease of photogenerated currents if compared to bare ZnO. It is suggested [27, 38, 39] that Co^{2+}/Co^{3+} ions can act as recombination centers for the photogenerated charge carriers thus reducing the overall performance of electrodes.

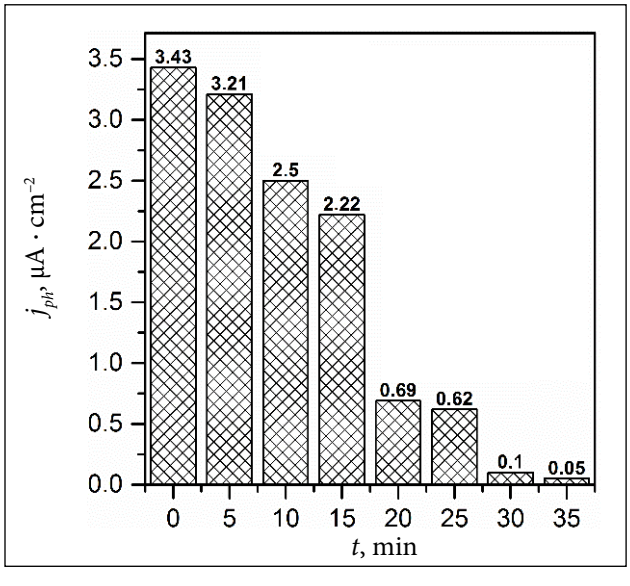

Fig. 8. Influence of the Co–P_i photodeposition time t on the photogenerated current of electrophoretically deposited ZnO coatings. E = +0.2 V, pH 11.5 phosphate electrolyte

It should be pointed out that, similarly to the WO_3/Co–P_i electrode [40], ZnO/Co–P_i showed an enhanced electrocatalytic activity in the dark, which increased with the increase in Co–P_i photodeposition time. However, the highest activity of the Co–P_i catalyst can be achieved at a potential which is more positive than 1 V. Under these conditions, the dissolution of stainless steel takes place, and for this reason, more stable ZnO/Co–P_i support, for example, electroconductive glass should be employed.

CONCLUSIONS

Nanostructured ZnO coatings on AISI 304 stainless steel were formed by electrophoretic deposition. It was revealed that the highest stability and photoactivity in the 0.1 M Na_2SO_4 solution is characteristic of the coatings synthesized under the following conditions: the electrophoresis potential of 30 V, the deposition time of 20 min and the amount of immobilized ZnO is 1.03 mg · cm^{-2}. The photovoltammetry measurements revealed that the obtained *n-type* ZnO films are highly photoactive in aqueous solutions under UV irradiation and the IPCE value at +0.6 V in 0.1 M Na_2SO_4 electrolyte is 14.6%. It was established that the increase in the amount of the Co–P_i catalyst decreases the observed photocurrent of the ZnO coatings; however, it simultaneously increases the electrocatalytic activity of anodic water oxidation.

Received 23 January 2017
Accepted 2 February 2017

References

1. H. Morkoç, Ü. Özgür, *Zinc Oxide. Fundamentals, Materials and Device Technology*, WILEY-VCH Verlag GmbH & Co. KGaA, Weinheim (2009).
2. C. Klingshirn, *Chemphyschem*, **8**, 782 (2007).
3. Ü. Özgür, Y. I. Alivov, C. Liu, et al., *J. Appl. Phys.*, **98**, 041301 (2005).
4. A. Moezzi, A. M. McDonagh, M. B. Cortie, *Chem. Eng. J.*, **185–186**, 1 (2012).
5. A. Kolodziejczak-Radzimska, T. Jesionowski, M. Maciejewska, et al., *Pol. J. Chem. Technol.*, **16**, 63 (2014).
6. R. van de Krol, M. Grätzel, *Photoelectrochemical Hydrogen Production*, Springer US, Boston, MA (2012).
7. Y. Surendranath, D. G. Nocera, in: *Progress in Inorganic Chemistry*, p. 505, John Wiley & Sons, Inc., New York (2011).
8. Y. Surendranath, M. W. Kanan, D. G. Nocera, *J. Am. Chem. Soc.*, **132**, 16501 (2010).
9. I. Corni, M. P. Ryan, A. R. Boccaccini, *J. Eur. Ceram. Soc.*, **28**, 1353 (2008).
10. Y. Hara, J. R. S. Brownson, M. A. Anderson, *Int. J. Appl. Ceram. Technol.*, **9**, 115 (2012).

11. E. M. Wong, P. C. Searson, *Chem. Mater.*, **11**, 1959 (1999).
12. F. Tang, Y. Sakka, T. Uchikoshi, *Mater. Res. Bull.*, **38**, 207 (2003).
13. F. Tang, T. Uchikoshi, Y. Sakka, *J. Am. Ceram. Soc.*, **85**, 2161 (2002).
14. Y. C. Wang, I. C. Leu, M. H. Hon, *J. Cryst. Growth*, **237–239**, 564 (2002).
15. Y. C. Wang, I. C. Leu, M. H. Hon, *J. Mater. Chem.*, **12**, 2439 (2002).
16. K. M. Wu, I. Zhitomirsky, *Int. J. Appl. Ceram. Technol.*, **8**, 920 (2011).
17. H.-W. Chen, C.-Y. Lin, Y.-H. Lai, et al., *J. Power Sources*, **196**, 4859 (2011).
18. X. Yin, X. Liu, L. Wang, et al., *Electrochem. Commun.*, **12**, 1241 (2010).
19. L. Miao, S. Cai, Z. Xiao, *J. Alloys Compd.*, **490**, 422 (2010).
20. J. H. Lee, I. C. Leu, Y. W. Chung, et al., *Nanotechnology*, **17**, 4445 (2006).
21. M. Verde, A. C. Caballero, Y. Iglesias, et al., *J. Electrochem. Soc.*, **157**, H55 (2010).
22. M. Verde, M. Peiteado, A. C. Caballero, et al., *J. Colloid Interface Sci.*, **373**, 27 (2012).
23. C.-C. Lin, Y.-Y. Li, *Mater. Chem. Phys.*, **113**, 334 (2009).
24. E. Valatka, Z. Kulesius, *J. Appl. Electrochem.*, **37**, 415 (2007).
25. L. V. Azároff, *Elements of X-ray Crystallography*, McGraw-Hill Book Company, New York (1968).
26. J. Georgieva, S. Armyanov, E. Valova, et al., *Electrochem. Commun.*, **9**, 365 (2007).
27. E. M. P. Steinmiller, K.-S. Choi, *Proc. Natl. Acad. Sci. U. S. A.*, **106**, 20633 (2009).
28. Y. Duan, J. Li, X. Yang, et al., *J. Anal. Appl. Pyrolysis*, **83**, 1 (2008).
29. R. A. Meyers, *Encyclopedia of Analytical Chemistry*, John Wiley & Sons, New York (2012).
30. T. Ishioka, Y. Shibata, M. Takahashi, et al., *Spectrochim. Acta, Part A*, **54**, 1827 (1998).
31. S. Vahur, A. Teearu, I. Leito, *Spectrochim. Acta, Part A*, **75**, 1061 (2010).
32. L. Besra, M. Liu, *Prog. Mater. Sci.*, **52**, 1 (2007).
33. K. Rajeshwar, in: A. J. Bard (ed.), *Encyclopedia of Electrochemistry*, WILEY-VCH Verlag GmbH & Co. KGaA, Weinheim (2007).
34. X. Domenech, J. A. Ayllon, J. Peral, *Environ. Sci. Pollut. R.*, **8**, 285 (2001).
35. P. Spathis, I. Poulios, *Corros. Sci.*, **37**, 673 (1995).
36. I. Betova, M. Bojinov, T. Laitinen, et al., *Corros. Sci.*, **44**, 2675 (2002).
37. R. Solarska, I. Rutkowska, R. Morand, et al., *Electrochim. Acta*, **51**, 2230 (2006).
38. M. W. Kanan, D. G. Nocera, *Science*, **321**, 1072 (2008).
39. Y. Wang, Y. Wang, R. Jiang, et al., *Ind. Eng. Chem. Res.*, **51**, 9945 (2012).
40. S. Ostachavičiūtė, R. Mardosaitė, E. Valatka, *Chemija*, **25**, 154 (2014).

Agnė Šulčiūtė, Simona Ostachavičiūtė, Eugenijus Valatka

ZnO DANGŲ ANT AISI 304 MARKĖS NERŪDIJANČIOJO PLIENO SINTEZĖ, STRUKTŪRA IR FOTOELEKTROCHEMINIS AKTYVUMAS

S a n t r a u k a

Termiškai skaidant cinko acetatą pagamintas nanostruktūrinis cinko oksidas ir elektroforezės metodu suformuotos jo dangos ant AISI 304 markės nerūdijančiojo plieno. Nustatyta, kad didžiausias fotoaktyvumas ir stabilumas 0,1 mol/l Na_2SO_4 tirpale būdingas dangoms, kurių sintezei tarp elektrodų taikyta 30 V įtampa, trukmė – 20 min., o nusodinto cinko oksido kiekis – 1,03 mg cm^{-2}. Rentgeno spindulių difrakcinės analizės rezultatai patvirtino, kad dangos sudarytos iš viurcito fazės cinko oksido, kurio kristalitų vidutinis dydis 35,3 nm. Siekiant padidinti gautų dangų fotoelektrokatalizinį aktyvumą, ZnO paviršiuje taikant fotocheminį metodą nusodintas kobalto fosfatinis ($Co–P_i$) katalizatorius. Nustatyta, kad didėjant $Co–P_i$ katalizatoriaus kiekiui ZnO dangose jų generuojamos fotosrovės vertės mažėja, tačiau vandens anodinės oksidacijos reakcijos metu didėja elektrokatalizinis aktyvumas.